LRP 648/99 October 1999

Applicability of the ballooning transform to trapped ions modes

G.L. Falchetto, J. Vaclavik, M. Maccio,
S. Brunner, L. Villard

Submitted for publication in
Physics of Plasmas

ISSN 0458-5895

Applicability of the ballooning transform to trapped ions modes

G.L. Falchetto*, J. Vaclavik, M. Maccio, S. Brunner[(a)], L. Villard

Centre de Recherches en Physique des Plasmas, Association Euratom-Confédération Suisse, Ecole Polytechnique Fédérale de Lausanne, PPB, CH-1015 Ecublens, Switzerland

[(a)] *Princeton Plasma Physics Laboratory, Princeton University,P.O. Box 451, Princeton, NJ 08543-0451, USA*

(October 13, 1999)

Abstract

In the scope of the study of low-frequency electrostatic microinstabilities in tokamak plasmas, attention has been focused on the effect of trapped ions. The ballooning transform has been applied to the gyrokinetic equation, for the case of a large aspect ratio plasma with circular magnetic surfaces. A new eigenvalue code has been developed to solve the resulting integral equation, for the case of adiabatic electrons and full ion dynamics, thus taking into account both circulating and trapped ions. The goal has been to assess the validity of the ballooning transform for trapped ion modes. A scan over the parameter $k_\theta \rho_L$ has been carried out to determine a lower threshold for applicability of the ballooning representation. Illustrative results of trapped ion modes (TIM) are presented, together with the comparison with the ones obtained using a global gyrokinetic code, for low toroidal wave numbers, and a local kinetic dispersion relation.

52.35.Kt, 52.25.Fi, 52.25.Dg, 52.35.-g

*E-mail: Gloria.Falchetto@epfl.ch

I. INTRODUCTION

Low-frequency microturbulence is commonly believed to be responsible for anomalous transport of heat and particles in tokamaks. Attention is focused here on ion temperature gradient (ITG) driven instabilities and in particular on the effects of trapped ion motion on such microinstabilities.

Previous linear calculations using the ballooning approximation did not deal with trapped ions modes (TIM) [1], [2]. Calculations including also the trapped ion effects have been done using a WKB approach, equivalent to the ballooning transform, in [3]. More recently global gyrokinetic calculations have shown the destabilizing effect of trapped ions [4], [5].

The aim of the present work has been to assess the validity of the ballooning representation [6], [7] to describe full ion dynamics, thus taking into account both circulating and trapped particles, for the limit case of low toroidal wave numbers and broad temperature profiles.

A general derivation of the eigenvalue equation in a toroidal, axisymmetric system, is given for a large aspect ratio, low β plasma. Electrons are considered adiabatic while the response of the ions is described by means of the gyrokinetic equation. Following the method presented by Dong et al. in [1], the ballooning transform has been applied to the gyrokinetic equation which is then solved separately for the two populations of circulating and trapped particles. The quasi-neutrality condition, which is the appropriate equation to describe low-frequency electrostatic perturbations, gives thus rise to a one-dimensional integral equation, which is numerically solved by means of the finite elements method. Technical details are presented in Sec. II. Alocal kinetic dispersion relation allowing to model the effects of trapped ions is also derived in Sec. II D, in order to provide a comparison.

The rest of the article is organized as follows. Sec. III provides some details on the numerical methods employed. Results from the ballooning calculations together with a comparison with the local kinetic dispersion relation and with computations from a global gyrokinetic spectral code [4], are presented in Sec.IV. Finally, the concluding remarks are drawn in Sec.V.

II. PHYSICAL MODEL

The effect of a low-frequency electrostatic perturbation on a low β tokamak plasma is studied. Attention is focused on the ion dynamics, described by means of the gyrokinetic equation , electrons being considered adiabatic. The quasi-neutrality condition provides the closure equation.

We consider an axisymmetric equilibrium with circular concentric magnetic surfaces; restraining the study to a large aspect ratio configuration, the magnetic field in usual toroidal variables (ρ, θ, φ) assumes the simple form:

$$\vec{B} = B\left(-\frac{\epsilon}{q_s}\,\vec{e}_\theta + \vec{e}_\varphi\right), \tag{1}$$

with amplitude $B = B_0\,(1 - \epsilon\cos\theta)$, B_0 being the magnetic field on the axis, $\epsilon = \rho/R \ll 1$ the inverse aspect ratio, R and $\rho \in [0, a]$ the major and minor radius of the tokamak; q_s is the safety factor. Applying this large aspect ratio approximation, only the lowest order non-vanishing terms with respect to ϵ are retained.

A. Gyrokinetic equation in ballooning approximation

The ballooning transform [8] has been applied to the electrostatic potential Φ:

$$\Phi(\rho, \theta, \varphi) = \sum_{p=-\infty}^{\infty} \hat{\Phi}(\rho, \theta + p2\pi)\ \exp\{i\ n\ S(\rho, \theta + p2\pi, \varphi)\}, \tag{2}$$

where $\theta + p2\pi \equiv \theta_b$ defines the ballooning angle or extended poloidal angle $(\theta_b \in \Re\ )$; n is the toroidal wave number and the eikonal function has the form $S = q_s(\rho)\,\theta_b + \varphi$.

Adopting the same formalism for the nonadiabatic part of the perturbed distribution function g, we obtain the gyrokinetic equation in ballooning representation, which, to the lowest order in ϵ, reads :

$$\left[\frac{\partial}{\partial t} - \frac{v_{\|}}{Rq_s}\frac{\partial}{\partial\theta_b} - ik_\theta v_{dz}\ (\cos\theta_b - \hat{s}\ \theta_b\ \sin\theta_b)\right]\ \hat{g}\,(\rho, \theta_b; t) =$$

$$= \left[\frac{q_i}{T_i}\,F_M\,\frac{\partial}{\partial t} + \frac{\partial F_M}{\partial\rho}\,\frac{ik_\theta}{B}\right]\ J_0\left(\frac{k_\perp v_\perp}{\omega_{ci}}\right)\ \hat{\Phi}(\rho, \theta_b; t). \tag{3}$$

Where $\hat{s}$ is the magnetic shear, v_{dz} is the magnetic drift velocity, F_M is the Maxwellian distribution function, $\omega_{ci} = q_i B/m_i$ is the ion cyclotron frequency and $\vec{k} = n\,\nabla S$.
Introducing the solution of the gyrokinetic ballooning equation into the quasi-neutrality equation , an integral Fredholm equation of the second kind is obtained, which is then solved by means of the finite elements method. Distinct approaches have to be used to solve equation (3) for circulating and trapped ions, the first having approximately constant parallel velocity $v_{||}$ while the velocity of the latter depends on the bouncing motion.
From now on, to simplify the notation of the ballooning angle, we will drop the subscript denoting it by θ.

B. Passing ions

To solve the gyrokinetic ballooning equation for circulating ions we considered parallel velocity as constant and we followed the method presented in the article by Dong et al. [1]. The nonadiabatic part of the perturbed ion density assumes the form of the following integral equation

$$\tilde{n}_i^P = \frac{q_i}{T_i} \int_{-\infty}^{\infty} d\theta'\, \mathcal{K}(\theta,\theta')\, \hat{\Phi}(\theta'), \tag{4}$$

the kernel of which, in dimensionless units, reads

$$\mathcal{K}(\theta,\theta') = -\frac{iu}{\sqrt{\pi}} \int_{-\infty}^{0} dt\; \frac{e^{-i\omega t}}{t}\; exp\left\{-\alpha\,\frac{u^2}{t^2}\,|\theta-\theta'|^2\right\}\; \frac{2}{1+\alpha}\; I_0\; exp\left\{-\frac{\gamma^2-\gamma'^2}{2(1+\alpha)}\right\}$$
$$\times\left[\omega + 1 - \frac{3}{2}\,\eta_i + \frac{2\eta_i}{1+\alpha}\left(1 + \frac{\gamma\gamma'}{1+\alpha}\,\frac{I_1}{I_0} - \frac{\gamma^2-\gamma'^2}{2(1+\alpha)}\right) + \eta_i\,\frac{u^2}{t^2}\,|\theta-\theta'|^2\right]. \tag{5}$$

To derive this expression we introduced a new variable:

$$t = -\frac{q_s R\,|\omega_{*i}|}{v_{ti}}\;\frac{|\theta-\theta'|}{v_{||}}, \tag{6}$$

where $\omega_{*i} = -(k_\theta\, T_i)/(q_i\, B\, L_n)$, L_n is the density gradient scale length and $v_{ti} = \sqrt{2T_i/m_i}$ is the ion thermal velocity. The other definitions we established in (5) are the following : $u = (k_\theta \rho_L\, q_s)/(\sqrt{2}\,\varepsilon_n)$, $\rho_L = v_{ti}/\omega_{ci}$ being the ions Larmor radius, $\varepsilon_n = L_n/R\,, \eta_i = L_n/L_{T_i}$,

$$\alpha = 1 + 2i\,\varepsilon_n\,\frac{(\sin\theta - \sin\theta'))(\hat{s}+1) - \hat{s}\,(\theta'\cos\theta' - \theta\cos\theta)}{\theta' - \theta},$$

$$\gamma \equiv \gamma(\theta) = \sqrt{2}\,k_\theta \rho_L \sqrt{1 + (\hat{s}\theta)^2}\,, \qquad \gamma' \equiv \gamma(\theta'), \tag{7}$$

I_0, I_1 are modified Bessel functions of argument $\left(\frac{\gamma\gamma'}{1+\alpha}\right)$. In previous expressions frequencies have been normalized to $|\omega_{*i}|$ and velocities to v_{ti} .

C. Trapped ions

For trapped ions the procedure to solve the gyrokinetic ballooning equation (3) is more complicated due to the fact that parallel velocity cannot be considered constant anymore and in particular changes its sign during the bouncing motion. We choose in that case a more convenient system of velocity space coordinates, $(\mathcal{E}, \kappa^2, \sigma)$, where $\mathcal{E}$ is the energy , σ the sign of parallel velocity and instead of the magnetic moment μ, we define:

$$\kappa^2 = \frac{\mathcal{E} - \mu B_0\,(1-\epsilon)}{2\mu B_0\,\epsilon},$$

In terms of these variables the trapped particles motion is confined between velocity reflection points or turning points $\theta_{1,2}$ corresponding to $\kappa^2 = \sin^2(\theta/2)$. In the ballooning formalism there is then an infinite number of pairs of turning points, so that for each θ only the surrounding pair has to be considered.

The nonadiabatic part of the trapped ion density in terms of our variables can formally be written:

$$\frac{T_i}{q_i}\,\tilde{n}_i^T = 2\pi \int_0^\infty d\mathcal{E} \int_0^1 d\kappa^2\, J_0\left(\zeta(\theta)\right)\, \mathcal{J} \sum_\sigma g_\sigma^T, \tag{8}$$

where g_σ^T is the nonadiabatic distribution function for trapped ions having velocity $\sigma|v_\parallel|$, J_0 is the Bessel function of zeroth order, having argument $\zeta(\theta) = 2k_\theta\rho_L\sqrt{\mathcal{E}(1 + (\hat{s}\,\theta)^2)}$ and $\mathcal{J}$ is the Jacobian of the transformation,

$$\mathcal{J} = \frac{\sqrt{\epsilon\,\mathcal{E}}}{(1 - \epsilon + 2\epsilon\kappa^2)^2\,\sqrt{\kappa^2 - \sin^2(\theta/2)}}\,.$$

To derive the solution of equation (3) we followed the method described in [2], making a variable transformation to a "quasi-time" ,

$$t(\theta) = 2\omega_b \int_{\theta_1}^{\theta} d\theta' \, \frac{Rq_s}{|v_{||}|} - \pi, \tag{9}$$

the advantage is that t is in this way defined in the interval $[-\pi, \pi]$; here $\omega_b = \pi\sqrt{\epsilon\,\mathcal{E}}/(2Rq_s\,K(\kappa))$ is the frequency of the trapped ion bouncing motion.

An explicit form for g_σ^T has been obtained for the chosen large aspect ratio configuration:

$$g_\sigma^T = F_M \, \frac{\omega - \omega^*}{2\omega_b} \sum_l \left\{ \exp\left\{ i\left(l\,t - \sigma R(\theta)\right)\right\} \frac{A_l^\sigma}{\Gamma + \sigma\, l} \right.$$

$$\left. - \frac{\sigma(-1)^l}{2\cos\pi\Gamma} \exp\left\{-i\sigma\ (\Gamma t + R(\theta))\right\} \left[\frac{A_l^+}{l+\Gamma} + \frac{A_l^-}{l-\Gamma} \right] \right\}. \tag{10}$$

This expression is in dimensionless form, energy $\mathcal{E}$ being normalized to v_{ti}^2 and frequencies to $|\omega_{*i}|$, so that $\omega^* = 1 + \eta_i(2\mathcal{E} - 3/2)$ while the normalized bounce frequency reads $\omega_b = \pi\sqrt{\epsilon\,\mathcal{E}}/(2u\,K(\kappa))$; u is defined as in the previous section.

In deriving (10) we made use of a Fourier series in terms of the variable t, the coefficients of which A_l^σ, are explicitly defined as

$$A_l^\sigma = \frac{1}{2\pi} \int_{-\pi}^{\pi} dt\ J_0(\zeta(\theta'(t)))\ e^{i\,\sigma\,R(\theta'(t))}\ \hat{\Phi}(\theta')\ e^{-i\,l\,t}$$

$$\equiv \frac{2\omega_b}{2\pi} \int_{\theta_1}^{\theta_2} d\theta' \, \frac{R\,q_s}{|v_{||}|}\ J_0(\zeta(\theta'))\ e^{i\,\sigma\,R(\theta')}\ \hat{\Phi}(\theta')\ e^{-i\,l\,t(\theta')}. \tag{11}$$

The other definitions introduced in (10) are listed below.

$$t(\theta) \equiv t(\hat{\theta}) = \pi\ \frac{F\,(\beta, \kappa)}{K(\kappa)}, \qquad \beta = \arcsin\left(\frac{1}{\kappa}\,\sin\frac{\hat{\theta}}{2}\right),$$

$$R(\theta) = \frac{k_\theta \rho_L q_s \sqrt{2\,\mathcal{E}}}{\sqrt{\epsilon}} \left[(2 + 4\hat{s}) \left(E\,(\beta, \kappa) - F\,(\beta, \kappa)\ \frac{E(\kappa)}{K(\kappa)} \right) - 2\hat{s}\,\theta\,\sqrt{\kappa^2 - \sin^2\,(\theta/2)} \right], \tag{12}$$

$$\Gamma = \frac{u}{\pi\sqrt{\epsilon\,\mathcal{E}}} K(\kappa)\,\omega + \frac{k_\theta \rho_L q_s \sqrt{2\,\mathcal{E}}}{\pi\,\sqrt{\epsilon}} \left[\left(4\hat{s}(\kappa^2 - 1) - 1 \right) K(\kappa) + (2 + 4\hat{s}) E(\kappa) \right].$$

$F(\beta, \kappa)$ and $E(\beta, \kappa)$, are elliptic integrals of the first and second kind, respectively, while $K(\kappa)$ and $E(\kappa)$ are the complete ones. In deriving previous expressions, we took advantage of the functional relations between the elliptic integrals which, for periodic amplitude of the integrals, allowed us to introduce again the poloidal angle, denoted by $\hat{\theta} \in [-\pi, \pi]$.

D. Local dispersion relation

To supply a comparison, a local kinetic dispersion relation has been derived from the quasi-neutrality equation . As we did for the ballooning case, we considered quasi-adiabatic electrons, while the nonadiabatic response of ions is the local solution of the gyrokinetic ballooning equation , obtained from (3) with the standard procedure of taking the local approximation $k_{\|} = -\frac{i}{Rq}(\frac{\partial}{\partial\theta})$.

The nonadiabatic part of the distribution function, h assumes then the form :

$$h = \frac{q_i}{T_i} F_M \frac{\omega - \omega_{*i}\left[1 + \eta_i(v^2/2 - 3/2)\right]}{\omega - \omega_{di} - k_{\|}v_{\|}} J_0\left(\frac{k_y v_\perp}{\omega_{ci}}\right) \hat{\Phi}(\theta), \tag{13}$$

with ω_{*i} defined as in previous subsections and

$$\omega_{di} = -\varepsilon_n \omega_{*i}\left(\frac{v_\perp^2}{2} + v_{\|}^2\right).$$

The resulting local kinetic dispersion relation, including also trapped ions, reads:

$$\left[1 + \tau - \tau\left(\alpha_P P^P + \alpha_T P^T\right)\right] = 0. \tag{14}$$

Here $\alpha_T \simeq \sqrt{2\epsilon}$ and $\alpha_P = 1 - \alpha_T$, are respectively the ratios of trapped and passing ions, and P^j is defined as follows

$$P^j = \frac{1}{\sqrt{2\pi}} \int_0^\infty dv_\perp v_\perp \int_{-\infty}^\infty dv_{\|}\, {J_0}^2(k_y v_\perp)\, e^{-v^2/2}\, \frac{\omega + k_y\left[1 + \eta_i(v^2/2 - 3/2)\right]}{\omega - \omega_{di} - \delta_j\, k_{\|}v_{\|}}, \quad {}_{j=P,T}, \tag{15}$$

with $\delta_P = 1$ and $\delta_T = 0$; the trapped particle effects are described by omitting the $k_{\|}v_{\|}$ term, which models bounce averaging. The expression above is in dimensionless units, velocities have been normalized to ion thermal velocity $v_{thi} = \sqrt{T_i/m_i}$, wave number $k_{\|}$ to L_n, k_y to ρ_L and frequencies to v_{ti}/L_n.

III. NUMERICAL METHOD

The eigenvalue integral equation resulting from quasi-neutrality equation has been numerically solved with the finite elements method. The integration interval has been discretized into a mesh of N equidistant points and the electrostatic potential $\hat{\Phi}$ projected on

a basis of linearly independent piecewise constant functions, $\{\psi_j(\theta)\}_{j=0,\cdots N}$.

The quasi-neutrality equation can then formally be written as:

$$\sum_{j=1}^{N} M_{kj}^{tot}(\omega)\,\phi_j = 0, \tag{16}$$

where the matrix M^{tot} is the sum over all species contributions,

$$M^{tot} = M^{electrons} + M^{adiab.\,ions} + \alpha_P\, M^{P\,ions} + M^{T\,ions}. \tag{17}$$

Here the nonadiabatic contribution of passing ions has been weighted by their fraction, $\alpha_P \simeq 1 - \sqrt{2\epsilon}$; as regards trapped ions, the nonadiabatic part of the density is automatically weighted, as integrations in velocity space have been performed only over the trapped particles domain, i.e. for values of $\kappa^2 : 0 < \kappa^2 < 1$.

The matrices for adiabatic electrons and of the adiabatic fraction of ions, read:

$$M^{electrons} = -\frac{1}{\tau}\, M^{adiab.\,ions}, \tag{18}$$

$$M_{kj}^{adiab.\,ions} = < k|\, j > \equiv \int_{-\infty}^{\infty} d\theta \int_{-\infty}^{\infty} d\theta'\; \psi_k(\theta)\, \psi_j(\theta') = \Delta\theta\, \delta_{kj}, \tag{19}$$

where $\tau = T_e/T_i$ and $\Delta\theta$ is the mesh step.

For the case of nonadiabatic passing ions, the discretization procedure is straightforward, projecting (4) on finite elements, leads to the matrix :

$$M_{kj}^{P\,ions} = < k|\, \mathcal{K}(\theta,\theta';\omega)\,|\, j > \equiv \int_{\theta_k}^{\theta_{k+1}} d\theta \int_{\theta'_j}^{\theta'_{j+1}} d\theta'\; \mathcal{K}(\theta,\theta';\omega). \tag{20}$$

The case of trapped ions is more delicate to treat. First of all, we computed equation (10) in the deeply trapped particles approximation, which corresponds to assume $\kappa \ll 1$ and $\theta \ll 1$, applying then the final expressions for all values of κ^2. Expanding in (12) the ballooning angle around $\theta_0 = p2\pi$ and the elliptic integrals for $\kappa \sim 0$, up to terms of the order $\mathcal{O}(\kappa^2)$, leads to the following expressions:

$$t(\hat{\theta}) = 2\arcsin\left(\frac{\hat{\theta}}{2\kappa}\right),$$

$$R(\theta) = \frac{k_\theta \rho_L q_s \sqrt{2\,\varepsilon}}{\sqrt{\epsilon}}\; \left[(2\hat{s}+1)(\hat{\theta}/2) - 2\hat{s}\;\theta\right]\; \sqrt{\kappa^2 - (\hat{\theta}/2)^2}, \tag{21}$$

$$\Gamma = \frac{u}{2\sqrt{\epsilon\,\varepsilon}}\,(1+\kappa^2/4)\,\omega + \frac{k_\theta \rho_L q_s \sqrt{\varepsilon}}{\sqrt{2\,\epsilon}}\,\left[(2\hat{s}-3/4)\kappa^2+1\right].$$

The deeply trapped ion density (8) has then been projected on finite elements, formally :

$$M_{kj}^{T\,ions} =< k|\,\tilde{n}_i^T\,|j>\,. \tag{22}$$

This operation involved the projection of Fourier coefficients (11) on finite elements:

$$A_l^\sigma = \frac{2\omega_b}{2\pi}\int_{\theta_1}^{\theta_2} d\theta'\,\frac{R\,q_s}{|v_\parallel|}\,J_0(\zeta(\theta'))\,e^{i\,\sigma\,R(\theta')}\,e^{-i\,l\,t(\theta')}\sum_{j=1}^{N}\psi_j(\theta')\,\phi_j \equiv \sum_{j=1}^{N} A_{l\,j}^\sigma\,\phi_j, \tag{23}$$

$$\begin{aligned} A_{l\,j}^\sigma &= \frac{2\omega_b}{2\pi}\int_{\theta'_j}^{\theta'_{j+1}} d\theta'\,\frac{R\,q_s}{|v_\parallel|}\,J_0(\zeta(\theta'))\,e^{i\,\sigma\,R(\theta')}\,e^{-i\,l\,t(\theta')} \\ &\equiv \frac{1}{2\pi}\int_{t(\theta'_j)}^{t(\theta'_{j+1})} dt\;J_0\left(\zeta(\theta'(t))\right)\,e^{i\,\sigma\,R(\theta'(t))}\,e^{-i\,l\,t}. \end{aligned} \tag{24}$$

The coefficients are finally rewritten for numerical implementation in terms of the poloidal angle, $\hat{\theta}$, so that the final form reads:

$$A_{l\,j}^\sigma = \frac{1}{2\pi}\int_{t(\hat{\theta}_j)}^{t(\hat{\theta}_{j+1})} dt\;J_0\left(\zeta(\hat{\theta}(t)+p2\pi)\right)\,\exp\left\{i\,\sigma\,R\left(\hat{\theta}(t)+p2\pi\right)\right\}\,e^{-i\,l\,t}. \tag{25}$$

Attention had to be paid to the integration intervals in the ballooning angle variable, as only the values included between turning points should be considered; although the discretization covered the whole poloidal domain, integrations have been performed only over finite elements falling internally to the couples of turning points, more precisely $\theta \subset [max(\theta_1,\theta_j), min(\theta_{j+1},\theta_2)]$.

IV. RESULTS

To assess the validity of the ballooning representation for TIM, we carried out a scan over the parameter $k_\theta \rho_L$ and we made a comparison with results from the local kinetic dispersion relation (14) and from global gyrokinetic computations [4].

We considered a deuterium plasma containing 63% of trapped ions.

The ballooning computations have been performed such that the modes fall in the trapped

ion regime, i.e. frequencies of the order of the average ion bounce frequency $\omega \sim< \omega_b >$. The chosen set of parameters is: $\epsilon = 0.2$, $\eta_i = 10.0$, $\tau = 1.0$, $\varepsilon_n = 1.0$, $\hat{s} = 1.0$, $q_s = 1.5$, for which $< \omega_b > \simeq 0.42$ (value normalized with respect to $|\omega_{*i}|/k_\theta \rho_L$.) The scan has been performed for values of $k_\theta \rho_L$ between 0.07 and 1.0.

Different eigenmode structures of TIM are plotted in Fig.1, for two values of the parameter, $k_\theta \rho_L = 0.9$ (frame a) and $k_\theta \rho_L = 0.07$ (frame b). Full and dashed lines respectively represent real and imaginary part of the electrostatic potential, as a function of the poloidal ballooning angle. It can be seen how for higher values of the parameter $k_\theta \rho_L$ the mode shows a good localization around $\theta_b = 0$ and is spanning the only fundamental interval $[-\pi, \pi]$. For low values, instead, the mode is more extended and its amplitude in the intervals surrounding the fundamental one, is comparable to the central amplitude, so that the mode starts to assume a periodic structure rather then ballooning . For the chosen set of parameters the value $k_\theta \rho_L = 0.07$ thus represents a threshold, beyond which ballooning looses its validity .

As regards the comparison with global results, it is first of all important to point out that global modes having different toroidal wave numbers and Larmor radii, but the same value of $k_\theta \rho_L = n q_s \rho_L / \rho$, are iso-dynamical in the frame of the lowest order ballooning approximation. As our purpose was to test the limits of applicability of the ballooning representation, we focused our attention to the case of low toroidal wave numbers, $n < 15$, and large Larmor radius. Some computations for an iso-dynamical case, having larger n and smaller Larmor radius, have been carried out for comparison.

Computations with the global gyrokinetic spectral code [4] , named GLOGYSTO, have been performed choosing the magnetic geometry (1) with: $R = 1.5\ m$, $a = 0.5\ m$ and a safety factor profile $q_s(s) = 1. + 2.315\, s^3$, $s = \rho/a$ being the normalized radial variable . The radial location corresponding to the chosen aspect ratio is $s_0 = 0.6$. Profiles have been chosen such that logarithmic derivatives are maximum at $s = s_0$; in particular, temperature profiles (identical for the two species) and density profiles have been taken of the form:

$$\frac{T(s)}{T_0} = \exp\left(-\frac{a\Delta s_T}{L_{T0}} \tanh\frac{s - s_0}{\Delta s_T}\right), \qquad \frac{N(s)}{N_0} = \exp\left(-\frac{a\Delta s_n}{L_{n0}} \tanh\frac{s - s_0}{\Delta s_n}\right), \tag{26}$$

with $\Delta s_T = 0.3$, $L_{T0} = 0.15\,m$, $\Delta s_n = 0.05$, $L_{n0} = 1.5\,m$. We would like to highlight that a particularly broad temperature gradient profile has been chosen to test limits of the ballooning approximation in the case of not very localized modes.

The iso-dynamical scenarios have been obtained considering two different values of magnetic field and T_0 (temperature at s_0) :

$$\begin{cases} B_0 = 1.\,\mathrm{T},\ T_0 = 5.\,\mathrm{keV} \ :\ \text{large Larmor radius},\ a/\rho_L = 48.94, \\ B_0 = 2.\,\mathrm{T},\ T_0 = 1.\,\mathrm{keV} \ :\ \text{small Larmor radius},\ a/\rho_L = 218.85. \end{cases} \tag{27}$$

Computations of the dispersion relation (14) were obviously performed choosing the same set of parameters as for ballooning ; moreover $k_{||} \simeq 1/Rq_s$.

The comparison of real frequencies and growth rates, normalized with respect to $|\omega_{*i}|/k_\theta \rho_L$, for the three codes is shown in Fig.2. The full line represents gyrokinetic ballooning results, dotted and dashed lines correspond to global gyrokinetic modes for the two iso-dynamical cases, respectively $a/\rho_L = 48.94$ and $a/\rho_L = 218.85$; labels above global modes symbols denote the values of the corresponding toroidal wave number. The local kinetic dispersion relation is drawn with a dash-dotted line.

The first remark to be made is that local computations show the presence of just one unstable mode, in the chosen regime, while from the global code distinct modes are found (for the small Larmor radius scenario, only the mode for which the growth rate peaks is shown). Good agreement between local and ballooning results is obtained. As regards global results, ballooning is able to better reproduce modes having higher toroidal wave number, as expected, while there is an evident discrepancy with the low n iso-dynamical scenario results: growth rates computed with the ballooning code are overestimated with respect to global ones of a factor $3-4$ for low n and $\simeq 1.7$ for high n. The discrepancy for very low values of n is of the same order as in the comparison presented in [9] for ITG modes without trapped ions. As regards the higher n global mode, the observed slight disagreement of ballooning results can be due to the high value of η_i, as previous studies on ITG showed a divergent behaviour of ballooning and global mode growth rates curves for increasing η_i [9] .

The growth rate peaks around $k_\theta \rho_L \simeq 0.5$ for both of the local results and around a slightly lower value for the global modes.

Some eigenmode structures, referring to the plot of Fig.2, are presented in the following figures. Fig.3 shows a comparison of the global mode $n = 3$ (frame a) and the most unstable global mode, $n = 8$ (frame b), for the iso-dynamical state $a/\rho_L = 48.94$. Plots on the left side show the radial dependence of poloidal mode Fourier components; on top axis the position of mode rational surfaces, for which $m = n\, q_s$, is reported. On the right side the mode structure in the poloidal plane, is shown. Those modes exhibit a typical TIM structure, i.e. only slightly ballooning and they are radially quite extended, being localized between magnetic surfaces $s = 0.4$ and $s = 0.8$. Note that the mode $n = 8$, compared with mode $n = 3$, is better centered around $s = s_0 = 0.6$ and coherent radial structures can be distinguished in the unfavorable curvature region, where the mode balloons.

Fig.4 highlights the different eigenmode structure for $k_\theta \rho_L = 0.66$ of a ballooning trapped ion mode (frame a) and the corresponding mode, obtained by only computing the circulating ions response (frame b). The values of normalized growth rates are respectively $\gamma = 0.465$, for the TIM and $\gamma = 0.535$, for the mode without trapped ions ($|\omega_{*i}|/k_\theta \rho_L = 3.26 \cdot 10^5 s^{-1}$). This points out that trapped ions have a stabilising effect , which is evident even for high values of $k_\theta \rho_L$, i.e. for frequencies well above the ion bounce frequency.

V. CONCLUSIONS

The effect of trapped ions on microinstabilities due to temperature gradients has been analysed by means of solving the gyrokinetic equation in ballooning approximation , for full ions dynamics. Differently from previous computations, the finite elements method, combined with a decomposition in a Fourier series, has been used to solve the resulting eigenvalue integral equation.

Results have been obtained from the new eigenvalue code. In particular the applicability of the ballooning transform to ion temperature gradient driven modes has been tested in

the limit case of low toroidal wave numbers and broad temperature gradient profiles; some computations for an iso-dynamical scenario with higher toroidal wave numbers have been done for benchmark.

Results from a scan over the parameter $k_\theta \rho_L$ proved that there is a lower threshold in $k_\theta \rho_L$, i.e. toroidal wave number, above which ballooning representation is applicable. Below this value, trapped ion modes become poloidally extended and the ballooning structure gives place to a nearly periodic one, so that the model is not valid anymore. In the region of parameters where ballooning is applicable there is anyway a discrepancy between mode growth rates obtained from the global and ballooning codes : with the ballooning representation growth rates are overestimated by a factor $\simeq 1.7$ for the higher n iso-dynamical scenario and by a factor $3-4$ for low toroidal wave numbers (in the regime of parameters we analyzed). For low values of n, this discrepancy is of the same order as in the comparison presented in [9] for only circulating ions.

We can then asses that local representations are able to qualitatively reproduce the full ion dynamics but for a more careful estimate of instability growth rates a global description seems to be necessary.

Acknowledgments

This work was partly supported by the Swiss National Science Foundation.

The computations have been performed on the Origin2000 of the EPFL.

REFERENCES

[1] J.Q. Dong, W. Horton and J.Y. Kim, Physics of Fluids B **4**(7), 1867, (1992)

[2] G. Rewoldt, W.M. Tang and M.S. Chance, Physics of Fluids **25**(3), 480, (1982)

[3] X. Garbet, L. Laurent, F. Morgues, J.P. Roubin, A. Samain, X.L. Zou and J. Chinardet, Physics of Fluids B **4**(1), 136, (1992)

[4] S. Brunner, M. Fivaz, T.M. Tran and J. Vaclavik, Physics of Plasmas **5**, 3929, (1998)

[5] M. Fivaz, Ph.D.Thesis, thesis 1692, Ecole Polytechnique Fédérale de Lausanne, Switzerland, (1997)

[6] J.W. Connor, R.J. Hastie and J.B. Taylor, Physical Review Letters **40**, 396, (1978)

[7] F. Pegoraro and T. Schep, Physics of Fluids **24**(3), 478, (1981)

[8] R.D. Hazeltine and W.A. Newcomb, Physics of Fluids B **2**(1), 7, (1990)

[9] S. Brunner, Ph.D.Thesis, thesis 1701, Ecole Polytechnique Fédérale de Lausanne, Switzerland, (1997)

FIGURE CAPTIONS

Fig.1 Comparison of eigenfunctions in terms of the poloidal ballooning angle for $k_\theta \rho_L = 0.9$ (a) and $k_\theta \rho_L = 0.07$ (b) . The other parameters are: $\epsilon = 0.2$, $\eta_i = 10.$, $\varepsilon_n = 1.$, $\tau = 1$, $\hat{s} = 1.$, $q_s = 1.5$.

Fig.2 Comparison of growth rates (a) and real frequencies (b) of trapped ions modes, as a function of $k_\theta \rho_L$, obtained from the gyrokinetic ballooning code (full line), the local kinetic dispersion relation (dash-dotted line) and the global gyrokinetic code for two iso-dynamical states: $a/\rho_L = 48.94$ (dotted lines) and $a/\rho_L = 218.85$ (dashed line). Labels above global modes symbols indicate the values of the corresponding toroidal wave number. In (b) only frequencies of the most unstable global modes, for the low n case are plotted; the high n iso-dynamical mode frequencies would be nearly superposed to open circles. Parameters of the ballooning code are the same as in Fig.1.

Fig.3 Comparison of eigenmode structures of global modes $n = 3$ (a) and $n = 8$ (b), referring to Fig.2 . Left plots show the radial dependence of poloidal mode Fourier components; top axis reports the position of mode rational surfaces, for which $m = n\, q_s$. Right plots show the structure in poloidal plane (dash-dotted lines represent the magnetic surfaces $s = 0.2, 0.4 \cdots$).

Fig.4 Comparison of eigenmode structures for the ballooning mode having $k_\theta \rho_L = 0.66$ with trapped ions (a) and without trapped ions (b). Normalized growth rates are respectively $\gamma = 0.465$ and $\gamma = 0.535$ ($|\omega_{*i}|/k_\theta \rho_L = 3.26 \cdot 10^5 s^{-1}$).

FIG.1 Falchetto

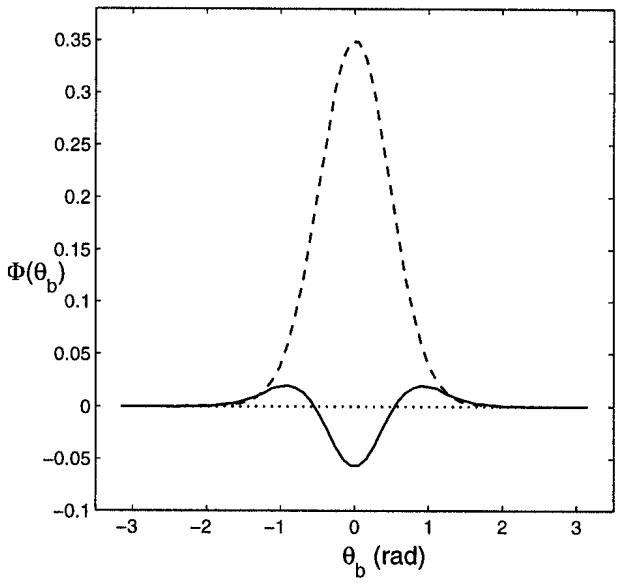

a.)

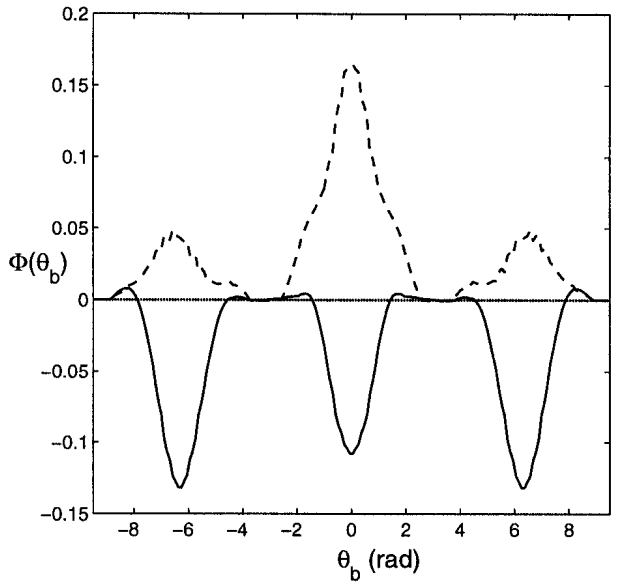

b.)

FIG.2 Falchetto

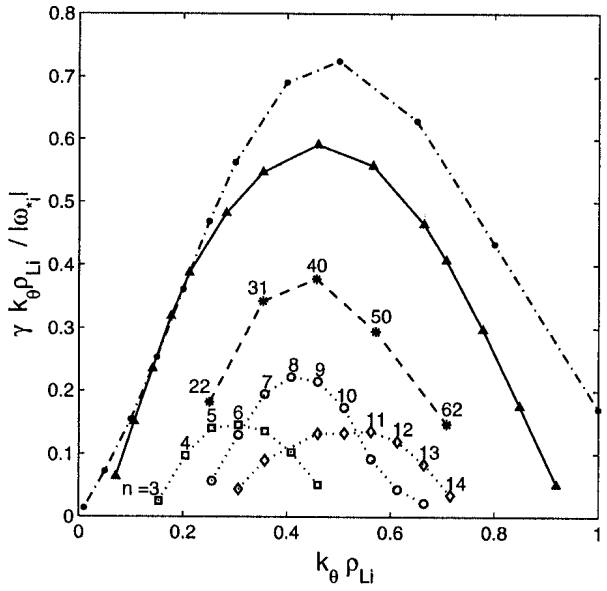

a.)

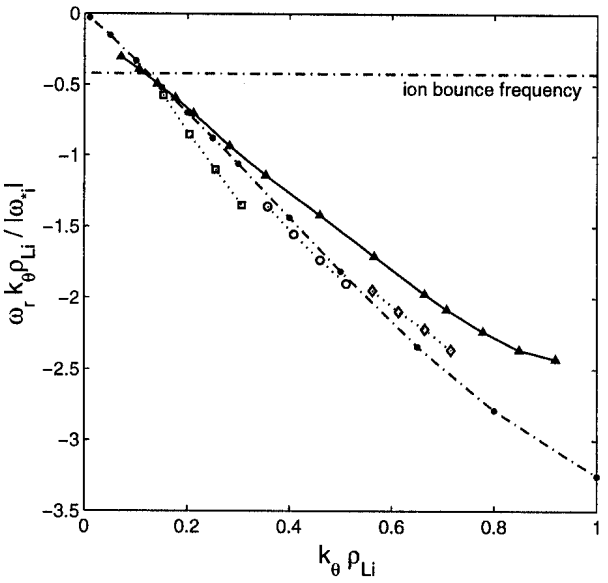

b.)

FIG.3 Falchetto

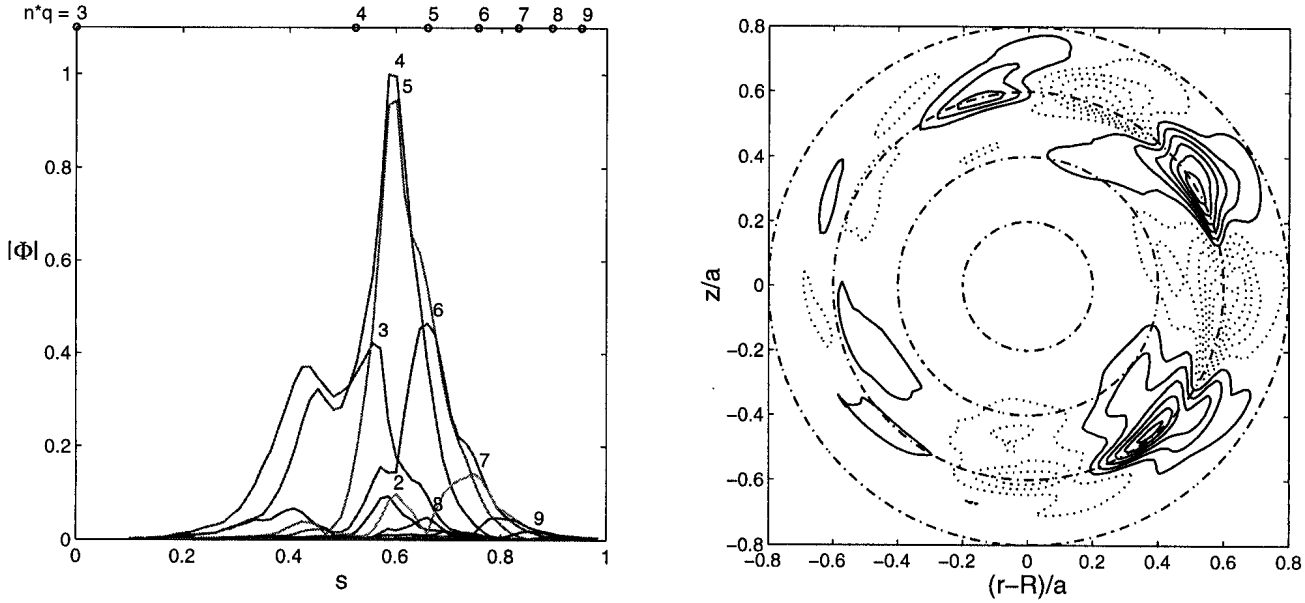

a.) $n = 3$

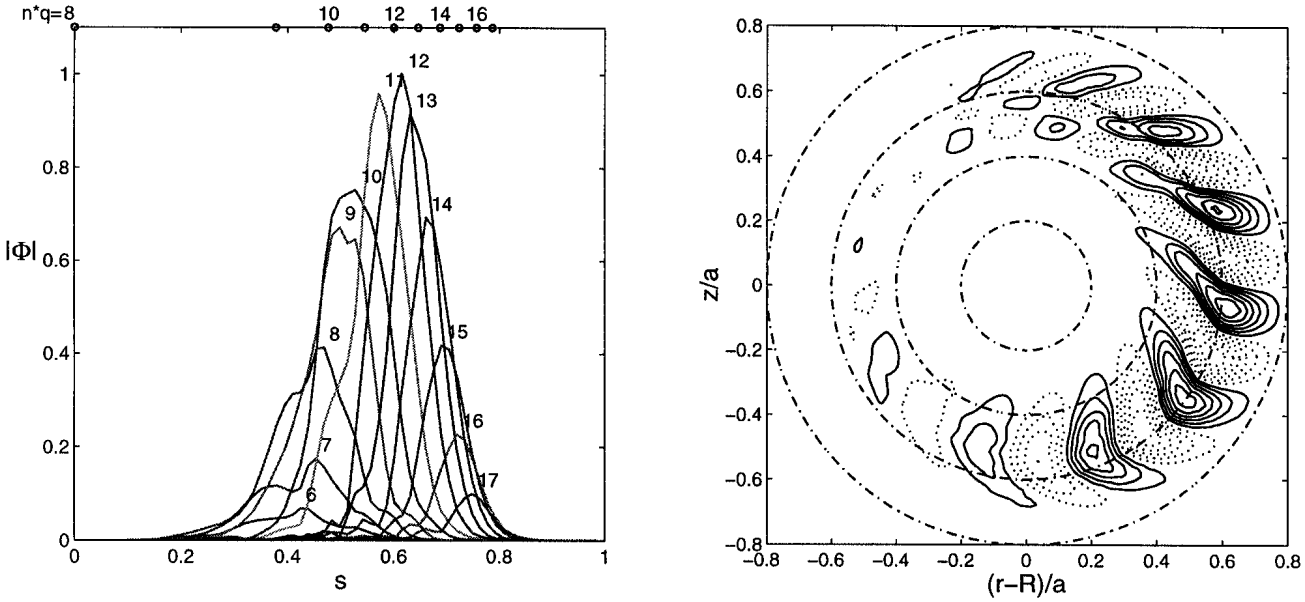

b.) $n = 8$

FIG.4 Falchetto

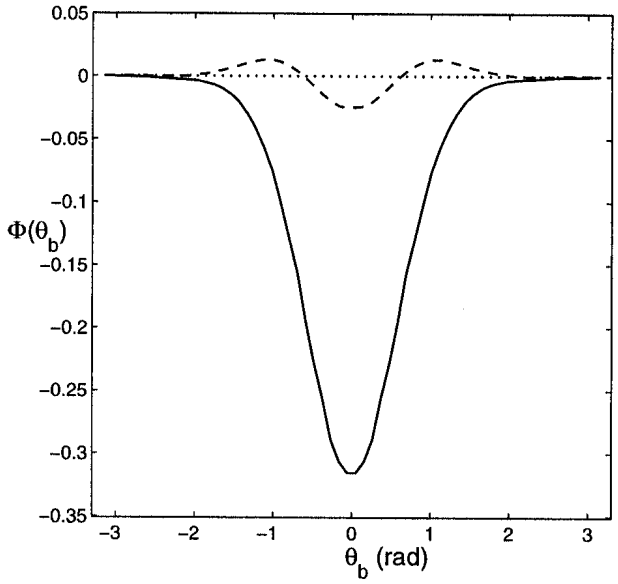

a.)

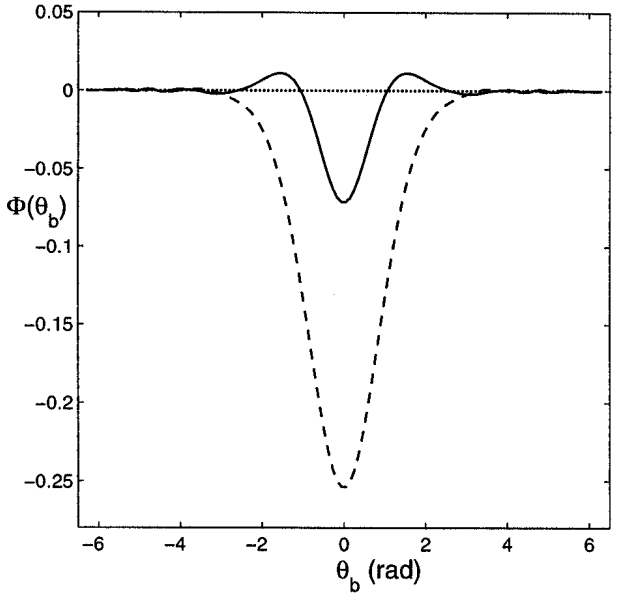

b.)